On the Combustion of Hydrogen−Rich Gaseous Fuels with Low Calorific Value in a Porous Burner

ARTICLE *in* ENERGY & FUELS · FEBRUARY 2010

Impact Factor: 2.79 · DOI: 10.1021/ef9010324

5 AUTHORS, INCLUDING:

Mário Costa
University of Lisbon
98 PUBLICATIONS **1,301** CITATIONS
SEE PROFILE

Rafael C. Catapan
Federal University of Santa Catarina
9 PUBLICATIONS **85** CITATIONS
SEE PROFILE

Energy Fuels **2010,** *24,* 880–887 · DOI:10.1021/ef9010324
Published on Web 12/30/2009

energy&fuels
article

On the Combustion of Hydrogen-Rich Gaseous Fuels with Low Calorific Value in a Porous Burner

R. W. Francisco Jr.,[†] F. Rua,[†] M. Costa,*[,†] R. C. Catapan,[‡] and A. A. M. Oliveira[‡]

[†]*Mechanical Engineering Department, Instituto Superior Técnico, Technical University of Lisbon, Avenida Rovisco Pais, 1049-001 Lisbon, Portugal, and* [‡]*Mechanical Engineering Department, Federal University of Santa Catarina, 88040-900 Florianópolis, SC, Brazil*

Received September 14, 2009. Revised Manuscript Received December 4, 2009

The main aim of this work is to investigate the combustion of hydrogen-rich gaseous fuels with a low calorific value in a porous burner, in particular, to study the effects of the composition of the fuel on flame stability and pollutant emissions. To this end, a range of low calorific value fuel gaseous mixtures of CH_4, H_2, CO_2, CO, and N_2 have been prepared in such a way that the constant pressure adiabatic flame temperature for all reacting mixtures was kept constant. In this study, the equivalence ratio was also kept constant. For comparison purposes, the combustion of pure methane in the same porous burner has also been studied. The results indicated that, for this burner design, the macroscopic flame shape of the fuel mixtures remains approximately the same as compared to pure methane but the former flames move further upstream from the burner exit. This is caused by the increase of the laminar flame speed as the H_2 content in the mixtures increases. As a result, the stability limits of the fuel mixture increase and the stability range enlarges. It was also observed that, for the Wobbe Index varying from 5 to 44 MJ/Nm^3, it is possible to burn stably at $\approx$260 kW/m^2, which reveals the fuel interchangeability potential of the present burner design. Because the flame moves further upstream, the enrichment with H_2 decreases the radiation efficiency. The pollutant emission indexes decreased significantly with the use of H_2-enriched mixtures. For all fuel mixtures, the maximum emission index of CO and NO_x was 0.75 and 0.09 g/kg, respectively.

1. Introduction

Low-calorific gaseous fuels can be produced as gas or waste fuel in steel production, refineries, petrochemicals, and other process industries, as biogas from anaerobic digestion of organic matter, and also as syngas from the thermal gasification of biomass, organic waste, and fossil fuels. Syngas from gasification of biomass is composed primarily of CO, H_2, CH_4, CO_2, N_2, and H_2O. Dependent upon the type of reactor and gasifying agent, lower heating values between 4 and 6 MJ/Nm^3 may be obtained, which are very low when compared to the value of 34 MJ/Nm^3 for pure CH_4. There is a strong drive nowadays to burn these mixtures in furnaces and gas turbines to increase the use of available fuels, especially renewable or waste fuels, to positively compensate for the atmospheric CO_2 inventory, or to avoid the emission of pollutants from flare systems.

The combustion of low-calorific gaseous fuels may present difficulties related to both flame stability and combustion efficiency.[1−7] Systems with high heat recirculation rates[8−10] can, however, increase the stability range and allow for an effective combustion of these fuels. One way of designing a burner with a high internal heat recirculation rate consists of inserting a porous medium in the flame region. This increases the heat transfer by conduction and radiation to regions upstream from the flame in a heat recirculation process. These burners show high temperature in the flame region, resulting in low CO and unburned hydrocarbon (HC) emissions and have the ability to operate at very lean equivalence ratios, contributing to attain low NO_x emissions. This type of burner has been extensively investigated,[9−26] and excellent reviews may be found in refs 8, 27, and 28.

*To whom correspondence should be addressed: Mechanical Engineering Department, Instituto Superior Técnico, Av. Rovisco Pais, 1049-001 Lisbon, Portugal. Telephone: +351218417372. Fax: +351218475545. E-mail: mcosta@ist.utl.pt.

(1) Giles, D. E.; Som, S.; Aggarwal, S. K. *Fuel* **2006**, *85*, 1729–1742.
(2) Chomiak, J.; Longwell, J. P.; Sarofim, A. F. *Prog. Energy Combust. Sci.* **1989**, *15*, 109–129.
(3) Tanaka, R.; Shinoda, M.; Arai, N. *Energy Convers. Manage.* **2001**, *42*, 1897–1907.
(4) Witton, J. J.; Noordally, E.; Przybylski, J. M. *Chem. Eng. J.* **2003**, *91*, 115–121.
(5) Adouane, B.; Hoppesteyn, P.; Jong, W.; Wel, M. V. D.; Hein, K. R. G.; Spliethoff, H. *Appl. Therm. Eng.* **2002**, *22*, 959–970.
(6) Berg, M.; Johansson, E. M.; Järas, S. G. *Catal. Today* **2000**, *59*, 117–130.
(7) Kusar, H. M. J.; Ersson, A. G.; Järas, S. G. *Appl. Catal., B* **2003**, *45*, 1–11.
(8) Wood, S.; Harris, A. T. *Prog. Energy Combust. Sci.* **2008**, *34*, 667–684.
(9) Weinberg, F. J. *Nature* **1971**, *233*, 239–241.
(10) Hardesty, D. R.; Weinberg, F. J. *Combust. Sci. Technol.* **1974**, *8*, 201–214.
(11) Takeno, T.; Sato, K. *Combust. Sci. Technol.* **1979**, *20*, 73–84.
(12) Kotani, Y.; Takeno, T. *Proc. Combust. Inst.* **1982**, *19*, 1503–1509.
(13) Yoshizawa, Y.; Kiyoshi, K.; Echigo, R. *Int. J. Heat Mass Transfer* **1988**, *31*, 311–319.
(14) Echigo, R. *ASME/JSME Therm. Eng. Proc.* **1991**, *4*, 21–32.
(15) Hsu, P.; Evans, W. D.; Howell, J. R. *Combust. Sci. Technol.* **1993**, *90*, 149–172.
(16) Khanna, V.; Goel, R.; Ellzey, J. L. *Combust. Sci. Technol.* **1994**, *99*, 133–142.
(17) Sahraoui, M.; Kaviany, M. *Int. J. Heat Mass Transfer* **1994**, *37*, 2817–2834.
(18) Mital, R.; Gore, J. P.; Viskanta, R. *Combust. Flame* **1997**, *111*, 175–184.
(19) Hackert, C. L.; Ellzey, J. L.; Ezekoye, O. A. *Combust. Flame* **1999**, *116*, 177–191.
(20) Brenner, G.; Pickenäcker, K.; Pickenäcker, O.; Trimis, D.; Wawrzinek, K.; Weber, T. *Combust. Flame* **2000**, *123*, 201–213.
(21) Lammers, F. A.; de Goey, L. P. H. *Combust. Flame* **2003**, *133*, 47–61.

A widely investigated design of the porous radiant burner[15,16,20,25,29,30] consists of a monolith formed by two distinct layers: a preheating region (PR) made of a porous matrix with a small pore size placed upstream and a stable-burning region (SBR) made of a porous matrix with a larger pore size placed downstream from the flow injection. A recently developed design employs discrete reactant injection orifices[29−31] to decrease the lean combustion limit and to enlarge the stability limits for combustion of lean mixtures, in both ambient and heated environments. The injection orifice generates a vertical jet of premixed reactants within the porous medium, resulting in a flame front with a conical shape and anchored around the rim of the injection orifice instead of at the interface between the PR and SBR layers. The stabilization mechanism is mostly fluidynamic, because the flame front position is strongly affected by both volumetric flow rate and equivalence ratio variations.[30]

The main aim of this work is to investigate the combustion of gaseous fuels with low calorific value in a porous burner, in particular, to study the effect of the composition of the fuel on flame stability and pollutant emissions. The present study evaluates the behavior of mixtures of CH_4, H_2, and CO diluted with CO_2 and N_2 while maintaining constant the adiabatic flame temperature at constant pressure. This was achieved by varying the mol fraction of CH_4 from 0 to 1 and calculating the mole fractions of the remaining components following $X_{CO} = (1 - X_{CH_4})/3$, $X_{H_2}=(1-X_{CH_4})/9$, $X_{CO_2}=(1-X_{CH_4})/9$, and $X_{N_2}=4\ (1 - X_{CH_4})/9$. Using α to denote the methane mole fraction in the gas fuel, the global combustion reaction with standard simplified dry air to saturate products for fuel lean mixtures can be represented as

$$\alpha CH_4 + \left(\frac{1-\alpha}{3}\right)CO + \left(\frac{1-\alpha}{9}\right)H_2 + \left(\frac{1-\alpha}{9}\right)CO_2 + 4\left(\frac{1-\alpha}{9}\right)N_2 + \left(\frac{4+23\alpha}{18}\right)\frac{1}{\phi}(O_2 + 3.76N_2) \rightarrow \left(\frac{4+5\alpha}{9}\right)CO_2 + \left(\frac{1+17\alpha}{9}\right)H_2O + \left[4\left(\frac{1-\alpha}{9}\right) + \left(\frac{4+23\alpha}{18}\right)\frac{3.76}{\phi}\right]N_2 + \left(\frac{4+23\alpha}{18}\right)\left(\frac{1}{\phi}-1\right)O_2 \quad (1)$$

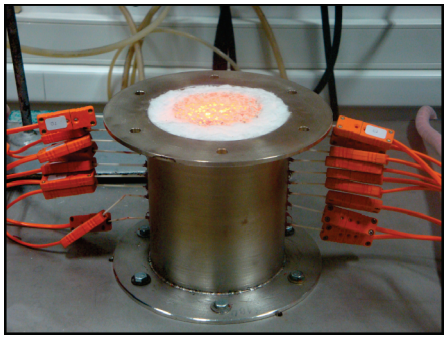

Figure 1. Photograph of the porous burner.

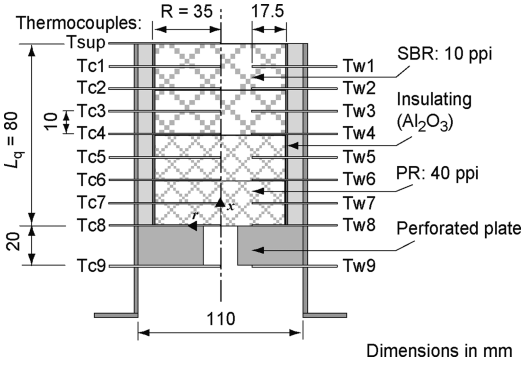

Figure 2. Schematic of the porous burner.

Table 1. Composition of the Ceramic Foams

element	content (%)
Al_2O_3	62.81
CaO	0.13
Fe_2O_3	0.24
MgO	0.08
MnO	0.02
Na_2O	0.01
P_2O_5	14.73
SiO_2	10.37
TiO_2	0.15
$ZrO_2 + HfO_2$	11.44

where ϕ is the fuel equivalence ratio and $0 \le \alpha \le 1$. In this work, the equivalence ratio was also kept constant ($\phi = 0.5$). This is most convenient because even with the increase in the heat content of the fuel, the heat content of the mixture remains the same by increasing the amount of air. As a result, the constant pressure adiabatic flame temperature for all of the gaseous fuels analyzed in this study is 1207 °C at $\phi = 0.5$ for reactants at 298 K and 1 atm. Therefore, the data can be analyzed knowing that they correspond to mixtures with essentially the same energy content, so that variations in combustion characteristics can be attributed mostly to chemical kinetics and to the interaction of the flame with the porous burner.

2. Experimental Section

2.1. Porous Burner. Figures 1 and 2 show a photograph and a rendering of the porous burner used in this work, respectively. The burner is made with four layers of porous foams, with 80% volumetric porosity, each with a diameter of 70 mm and a thickness of 20 mm. Table 1 shows the composition of the porous foams measured by X-ray fluorescence (XRF) and atomic absorption spectroscopy (AAS). The ceramics used are mostly composed of alumina (above 60%), with smaller proportions of phosphorus, zircon, and other oxides. As shown in

(22) Hayashi, T. C.; Malico, I.; Pereira, J. C. F. *Comput. Struct.* **2004**, *82*, 1543–1550.
(23) Talukdar, P.; Mishra, S. C.; Trimis, D.; Durst, F. *J. Quant. Spectrosc. Radiat. Transfer* **2004**, *84*, 527–537.
(24) Barra, A. J.; Ellzey, J. L. *Combust. Flame* **2004**, *137*, 230–241.
(25) Delalic, N.; Mulahasanovic, D.; Ganic, E. N. *Exp. Therm. Fluid Sci.* **2004**, *28*, 185–192.
(26) Pereira, F. M.; Oliveira, A. A. M.; Fachini, F. F. *Combust. Flame* **2009**, *156*, 152–165.
(27) Howell, J. R.; Hall, M. J.; Ellzey, J. L. *Prog. Energy Combust. Sci.* **1996**, *22*, 121–145.
(28) Oliveira, A. A. M.; Kaviany, M. *Prog. Energy Combust. Sci.* **2001**, *27*, 523–545.
(29) Catapan, R. C.; Pereira, F. M.; Oliveira, A. A. M. Development of a porous radiant burner with a combined thermal and fluidynamic mechanism of flame stabilization. Proceedings of the 18th International Congress of Mechanical Engineering, COBEM 2005, Ouro Preto, Brazil, Nov 6−11, 2005.
(30) Catapan, R. C.; Oliveira, A. A. M.; Costa, M. Fluidynamic mechanism of flame stabilization in a porous radiant burner. Manuscript submitted for publication.
(31) Francisco, R. W., Jr.; Rua, F.; Costa, M.; Catapan, R. C.; Oliveira, A. A. M. Combustion of low calorific value gaseous fuels in a porous burner: Effect of the fuel composition on flame stability and pollutant emissions. Proceedings of the 10th International Conference on Energy for a Clean Environment, Lisbon, Portugal, 2009.

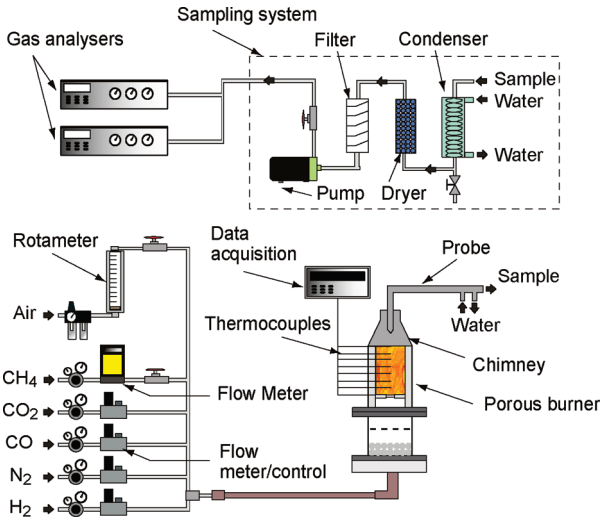

Figure 3. Schematic of the experimental setup.

Figure 2, the PR comprises two layers with 40 pores per inch (ppi) and the SBR contains two layers with 10 ppi. An injection plate with a single central orifice with 16 mm in diameter is placed under the PR. The use of this type of orifice produces a regime of combustion in which a flame burns stably over a large stability range for a given equivalence ratio.[30]

2.2. Experimental Setup and Techniques. Figure 3 shows a schematic of the experimental setup. The fuel supply system is composed of bottles of pressurized gases, a reducing-control valve, and a check valve. The gases include 99.8% pure CH_4, 99.997% pure CO, 99.995% pure CO_2, 99.999% pure H_2, and 99.999% pure N_2. Electronic flow meters connected to control valves were used for measuring and controlling the flow rate of the gases.

The air supply system is composed of an alternative compressor connected to a storage tank, a filter, a reducing valve, a check valve, a flow control valve, and a flow meter. During the tests, the air pressure at the tank was kept at 4 atm, while the burner operated under atmospheric pressure. The gaseous fuels and the air were fed to the burner through a stainless-steel pipe of 1 m in length and 25 mm in diameter, which homogenized the reactant mixture before reaching the burner.

The temperatures within the porous burner were measured with the aid of 18 R-type thermocouples (Pt/Pt−13% Rh) made with 250 μm diameter wires placed inside alumina double-holed tubes with a diameter of 1.59 mm. The thermocouples were positioned at $r/R = 0$ and 0.5 (see Figure 2, where R is the ceramic foam radius) and connected to a data acquisition system interfaced with a computer. Because of the thermal equilibrium established between the thermocouple hot junction, the gas, and the solid phase, the measurements provided by this sensor should be understood as a mean temperature between the gas and the solid phases.

A chimney was placed at the top of the burner to homogenize the flue gas and to facilitate sampling. The combustion products were sampled with the aid of a water-cooled stainless-steel probe for the measurement of O_2, CO, CO_2, HC, and NO_x concentrations. Before reaching the analyzers, the sample was cleaned and dried. The analytical instrumentation included a magnetic pressure analyzer for O_2 measurements, non-dispersive infrared gas analyzers for CO and CO_2 measurements, a flame ionization detector for HC measurements, and a chemiluminescent analyzer for NO_x measurements. Zero and span calibrations with standard mixtures were performed before and after each daily session. The maximum drift in the calibration was within ±2% of the full scale. In the postflame region, probe effects are negligible and errors arise mainly from quenching of chemical reactions, sample handling, and analysis. Our best estimates have indicated uncertainties of less than 8% for the concentrations of the gas species in the postflame region. Repeatability of the postflame gas species concentration data was, on average, within 5%.

2.3. Experimental Procedure. Initially, a near stoichiometric mixture is set, and the flame is ignited at the burner top. The flame front penetrates quickly into the porous medium reaching the PR, as indicated by a temperature rise in thermocouple Tc6 (see Figure 2). This initial heating process takes around 10 min. Subsequently, the desired test condition is set, and the flame propagation is observed. The flame is considered stable when the temperatures remain constant for at least 20 min.

The flame stability limits were determined by keeping the equivalence ratio constant and varying the total mass flow rate in small increments. The lower stability limit was defined as the mass flow rate at which the flame front reaches the position of thermocouple Tc7 (see Figure 2), located in the PR. Below this limit, the injection plate reaches its degradation temperature. The upper stability limit was defined as the mass flow rate at which flame detachment occurs and is visually observed as a blue flame floating on the burner surface. In general, the lift off occurs in the central region of the burner surface for the experimental conditions analyzed in this work. The maximum equivalence ratio used was limited by the maximum temperature supported by the porous media. For the ceramic foams used in this work, we observed that temperatures above 1600 °C resulted in a change in the structure evidenced by a color change and the appearance of vitrified points. Thus, the maximum temperature allowed was set in 1550 °C. This temperature occurs near the tip of the conical flame.

3. Results and Discussion

This section is divided into three subsections: subsection 3.1 presents a laminar-free flame analysis, including the effect of increasing the H_2 content in the fuel mixture; subsection 3.2 analyzes the flame stability limits and the pollutant emissions for pure methane; and finally, subsection 3.3 examines the flame stability limits and the pollutant emissions for the fuel mixtures for a constant adiabatic flame temperature of 1207 °C and a constant equivalence ratio of 0.5.

Table 2 presents the characteristics along with some properties of the fuel mixtures used. The properties presented include the molar mass (M_f), density (ρ_f), lower heating value (LHV), higher heating value (HHV), Wobbe Index (WI), fuel mass fraction in the reactant mixture ($Y_{f,n}$), mean constant pressure specific heat (c_p), constant pressure adiabatic flame temperature (T_{ad}), and the unstretched laminar flame speed (burning velocity, S_L), at $\phi = 0.5$, predicted by ChemKin 3.6,[32] for the reaction with standard simplified dry air at 298 K and 1 atm, using GRIMech 3.0.[33] The H/C and C/O ratios were kept between 0.5 and 4.0 and 0.8 and infinity (no oxygen in the fuel), respectively, for the fuel mixtures.

The range of LHV (or WI) of the mixtures established and studied includes fuels with low heating values (LHV from 3 to 7.9 MJ/m^3 at 298 K and 1 atm) that are typical of landfill, synthesis, residual, and waste gases and with high heating values (LHV from 23.6 to 63 MJ/m^3 at 298 K and 1 atm),

(32) Kee, R. J.; Rupley, F. M.; Miller, J. A.; Coltrin, M. E.; Grcar, J. F.; Meeks, E.; Moffat, H. K.; Lutz, A. E.; Dixon-Lewis, G.; Smooke, M. D.; Warnatz, J.; Evans, G. H.; Larson, R. S.; Mitchell, R. E.; Petzold, L. R.; Reynolds, W. C.; Caracotsios, M.; Stewart, W. E.; Glarborg, P.; Wang, C.; Adigun, O. CHEMKIN Collection, Release 3.6, Reaction Design, Inc., San Diego, CA, 2000.

(33) Smith, G. P.; Golden, D. M.; Frenklach, M.; Moriarty, N. W.; Eiteneer, B.; Goldenberg, M.; Bowman, C. T.; Hanson, R. K.; Song, S.; Gardiner, W. C., Jr.; Lissianski, V. V.; Qin, Z. GRIMech 3.0, available at http://www.me.berkeley.edu/gri_mech/.

Table 2. Properties of the Fuel Mixtures Used

fuel mixture	1	2	3	4	5	6	7
			Composition (Volume %)				
CH_4	0	10	20	40	60	80	100
CO	33.3	30	26.7	20	13.3	6.7	0
H_2	11.1	10	8.9	6.7	4.4	2.2	0
CO_2	11.1	10	8.9	6.7	4.4	2.2	0
N_2	44.4	40	35.6	26.7	17.8	8.9	0
H/C	0.5	1.2	1.8	2.6	3.2	3.7	4
C/O	0.8	1.0	1.3	2.0	3.5	8.0	
			Properties				
M_f (kg/kmol)	26.9	25.8	24.7	22.6	20.4	18.2	16.0
ρ_f (kg/m^3)	1.1	1.055	1.011	0.922	0.833	0.745	0.656
LHV (kJ/m^3)	4954	7738	10522	16091	21659	27227	32795
HHV (kJ/m^3)	5154	8287	11401	17648	23896	30143	36390
WI[a] (MJ/m^3)	5	8	11	18	26	34	44
$Y_{f,n}$[b] (kg/kg)	0.306	0.190	0.135	0.081	0.054	0.039	0.028
c_p[c] (kJ/kg K)	1.16	1.18	1.19	1.19	1.20	1.20	1.20
T_{ad}[d] (°C)	1208.8	1207.5	1206.9	1206.3	1206.0	1205.8	1205.7
S_L[e] (cm/s)	7.3	10.8	8.5	6.4	5.5	5.0	4.8

[a] WI calculated with LHV at 298 K and 1 atm, using $\rho_{air} = 1.17$ kg/m^3. [b] Mass of fuel per mass of reactant mixture for combustion with standard simplified dry air at $\phi = 0.5$. [c] Mean constant pressure specific heat between T_o and T_{ad}. [d] Constant pressure adiabatic flame temperature considering full species equilibrium in GRIMech 3.0. [e] Unstretched laminar flame speed predicted by ChemKin 3.6, using GRIMech 3.0, at 298 K and 1 atm.

Table 3. Summary of the Range of Conditions and Methods Used To Measure and Predict the Laminar Flame Speed for CH_4, H_2, CO, CO_2, and N_2 Mixtures in Combustion with Dry Air

	fuel mixture composition (volume %)						predictions			
reference	CH_4	H_2	CO	CO_2	N_2	measurements[a]	kinetics[b]	ϕ	T_u (K)	P (atm)
34	80−100	0−20				SCVR	GRIMech 3.0	0.7−1.0	298	1−5
36		5	95	10		BB, SF	GRIMech 3.0, H_2/CO mechanism	0.6−1	300−700	1−15
		50	50	20						
		95	5	40						
		23−38			62−77[c]					
37	0−9	15−21	22−25			SCVR, $\phi = 0.8$−1.6, 300 K, 1 atm	GRIMech 3.0	0.8−1.6	300−2300	1−50
38	20−100			0−80			GRIMech 3.0	1	298	1
	10−100				0−90					
		5−40	10	5	45−80			0.67, 0.77, 1	273, 773	
	0−20	8	10−30	12	50					
39	3.5	10.7	14.2	14.2	55.2	BB, $\phi = 0.86$, 300 K, 400 K, 1 atm	GRIMech 3.0	0.5−1.2	300−850	0.1−1.52

[a] Measurement methods: BB, Bunsen burner; SF, stagnation flow; SCVR, spherical constant volume reactor. [b] Mechanisms: GRIMech 3.0[33] and H_2/CO mechanisms.[41] [c] The authors burned 100% H_2 with a synthetic air formed by 10% O_2/90% N_2 at $\phi = 0.8$, 1.0, and 1.6.

which are equivalent to natural gas. Combustion systems can usually burn fuels within a 10% variation in the WI without any adjustment of the control systems or injector orifices. Note that the WI values in Table 2 vary by almost 10 times. The concentration of the inert components (N_2 and CO_2) varies from 11 to 55%. The CO/H_2 mole ratio is kept equal to 3.

3.1. Laminar-Free Flame Analysis. The measurement and calculation of the unstretched laminar flame speed for mixtures of CH_4, H_2, CO, CO_2, N_2, and O_2 have been studied in connection with the use of natural gas and alternative fuels for power production.[34−41] Because the H_2, CO, and CH_4 mechanisms form the basis over which mechanisms for heavier hydrocarbon are built, the more comprehensive studies[40,41] have increased the understanding of the basic chemical kinetic paths in hydrocarbon combustion and the predictive capability of the available detailed chemical kinetic models. Table 3 summarizes the range of conditions and methods used to measure and predict the laminar flame speed for CH_4, CO, and H_2 mixtures.[34−39] In general, the results indicate that an increase in the H_2 concentration usually increases the flame speed, with the effect being stronger for rich mixtures ($\phi > 1$) and lower CH_4 concentrations. Halter et al.[34] showed that, for CH_4/H_2/air mixtures at $\phi = 1.2$, a variation in the H_2 mole faction from 0 to 0.2 caused a 50% increase in S_L, while this increase was about 10% for $\phi = 0.7$. De Goey et al.[35] using a flame asymptotic analysis for CH_4/H_2/air flames at $\phi = 1.0$ and a skeletal mechanism showed that the inner layer structure remains about the same when CH_4 is replaced by H_2. The extra

(34) Halter, F.; Chauveau, C.; Djebaïli-Chaumeix, N.; Gökalp, I. *Proc. Combust. Inst.* **2005**, *30*, 201–208.
(35) de Goey, L. P. H.; Hermanns, R. T. E.; Bastiaans, R. J. M. *Proc. Combust. Inst.* **2007**, *31*, 1031–1038.
(36) Natarajan, J.; Nandula, S.; Lieuwen, T.; Seitzman, J. Laminar flame speeds of synthetic gas fuel mixtures. Proceedings of GT2005, American Society of Mechanical Engineers (ASME) Turbo Expo 2005: Power for Land, Sea and Air, Reno−Tahoe, NV, 2005.
(37) Hernandez, J. J.; Lapuerta, M.; Serrano, C. *Energy Fuels* **2005**, *19*, 2172–2178.
(38) Al-Hamamre, Z.; Diezinger, S.; Talukdar, P.; Von Issendorff, F.; Trimis, D. *Process Saf. Environ. Prot.* **2006**, *84*, 297–308.
(39) Ouimette, P.; Seers, P. *Fuel* **2009**, *88*, 528–533.
(40) Dagaut, P.; Dayma, G. *Int. J. Hydrogen Energy* **2006**, *31*, 505–515.
(41) Davis, S. G.; Joshi, A. V.; Wang, H.; Egolfopoulos, F. *Proc. Combust. Inst.* **2005**, *30*, 1283–1292.

amount of H_2 is consumed in the oxidation layer. The temperature of the inner layer decreases and the adiabatic flame temperature increases as CH_4 is replaced by H_2. As a result, the adiabatic flame temperature increases almost linearly with X_{H_2}/X_{CH_4}. Predictions using GRIMech[33] confirmed the findings from the asymptotic theory. In most of the laminar flame studies,[34−41] flame speeds were predicted using the Premix code from ChemKin[32] with both the GRIMech 3.0[33] and the Davis et al.[41] H_2/CO mechanisms. Both mechanisms provided relative good qualitative predictions. A sensitivity analysis[37] on the flame speed at 300 K and 1 atm using GRIMech 3.0[33] for a mixture with 3.5% CH_4, 25% CO, and 21% H_2 showed that the $OH + CO \leftrightarrow H + CO_2$ reaction is the most sensitive followed by the reactions $H + O_2 \leftrightarrow O + OH$, $H + HO_2 \leftrightarrow 2OH$ and $O + H_2 \leftrightarrow H + OH$ (reactions involving CH_3 are less important), which follows the trends observed by Davis et al.[41] These authors showed the importance of the $OH + CO \leftrightarrow H + CO_2$ reaction and the difficulty in finding a single Arrhenius expression valid for the whole range of interest. However, for conditions outside the target regions for which the mechanisms have been optimized,[33,41] the quantitative predictions were poor. This was observed for (1) pure H_2 highly diluted with N_2 (70% N_2) (the deviations increased well above 50% for equivalence ratios below 0.9),[36] and (2) for mixtures with a low content of CH_4 (3.5% CH_4) diluted with N_2 (50%) for equivalence ratios below 0.8.[39]

The reactant mixtures studied in the present work are much leaner when compared to the mixtures studied previously (Table 3) and are outside the original targets for which the GRIMech 3.0[33] and the Davis et al.[41] H_2/CO mechanisms were developed. This could lead to significant deviations in the predicted flame speeds, as noted above. Nevertheless, in the absence of flame speed measurements, the GRIMech 3.0[33] mechanism was used in the ChemKin 3.6[32] code for the prediction of the free, unstretched, laminar flame speed at 298 K and 1 atm, for the mixtures studied here, as presented in the last row of Table 2. Convergence was achieved starting with a stoichiometric CH_4/air premixed flame, then successively decreasing the equivalence ratio, and finally, changing the composition at $\phi = 0.5$. We note, however, a peculiar behavior in the flame speed values listed in Table 2. For 0% CH_4, the flame speed predicted with GRIMech 3.0[33] was 7.3 cm/s, which is smaller than the flame speed predicted for 10% CH_4. Using the mechanism of Davis et al.,[41] a value of 8.4 cm/s was obtained. This H_2/CO mechanism was built using GRIMech 3.0[33] as one of the basic sources. Even with the optimization of the rates of some of the important reactions, the results are very close. At the moment, we offer no explanation why these values are smaller than the value obtained for 10% CH_4. Therefore, in the absence of measurements, these estimates should be used with caution.

3.2. Flame Stability Limits and Pollutant Emissions for Pure Methane. Figure 4 presents the flame stability limits for pure methane. The figure represents the mean flow velocity, u_{ch}, defined as the volumetric flow rate of reactants divided by the transversal sectional area of the burner, as a function of the equivalence ratio, ϕ. For stationary plane flames, the mean flow velocity is equal to the flame speed. However, for the present burner, the flame has a conical shape and the equilibrium between the reactant flow velocity and the burning velocity is reached only locally. Three different regions can be identified, namely, the lift off region (above the upper stability limit), the stable flame region, and the thermal damage region (below the lower stability limit). The continuous lines identify the upper and lower burner stability limits.

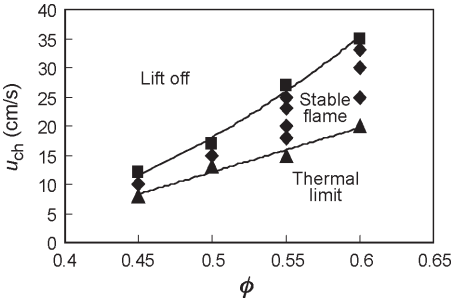

Figure 4. Flame stability limits for pure methane.

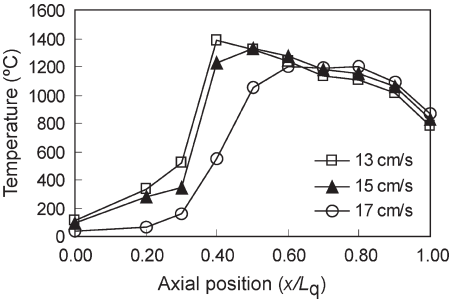

Figure 5. Temperatures along the center of the porous medium with pure methane for $\phi = 0.50$ for different mean flow velocities.

The burner power varied between 0.45 kW (117 kW/m^2) for a flame with $\phi = 0.45$ and $u_{ch} = 8$ cm/s and 2.74 kW (712 kW/m^2) for a flame with $\phi = 0.60$ and $u_{ch} = 35$ cm/s. This implies a turn-down ratio of about 6:1. Tests above $\phi = 0.60$ were not conducted because of the possibility of burner degradation.

Figure 5 shows the measured temperatures along the centerline of the porous medium for $\phi = 0.50$ for different mean flow velocities. The flame region can be identified as the position where the temperature reaches the highest values. It is seen that increases in the mean flow velocity cause the flame to move downstream. Also, the maximum measured temperature is ≈1380 °C for $u_{ch} = 13$ cm/s, which is about 180 °C higher than the constant pressure adiabatic flame temperature.

Figure 6 shows the radiation efficiency for pure methane as a function of the mean flow velocity for different equivalence ratios. The radiation efficiency is defined here as

$$\eta_{rad} = \varepsilon\sigma(T_{sup}^4 - T_\infty^4)/\dot{V}_F \mathrm{LHV} \quad (2)$$

where ε is the emissivity of the burner surface (assumed equal to the unit), σ is the Stefan−Boltzmann constant, and $\dot{V}_F$ is the fuel volumetric flow rate. T_{sup} was measured by the thermocouple placed on the center of the burner surface (Figure 2). The radiation efficiency varied between 26 and 39%. Catapan et al.[30] investigated a porous burner using similar porous foam and measured values for the radiation efficiencies between 20 and 30%. As from Catapan et al.,[30] Figure 6 reveals that higher equivalence ratios yield lower radiation efficiencies.

Figure 7 shows the emission index (EI) of CO for pure methane as a function of the mean flow velocity for different equivalence ratios. The EI of a pollutant stands for the ratio between the mass of the component yielded and the total

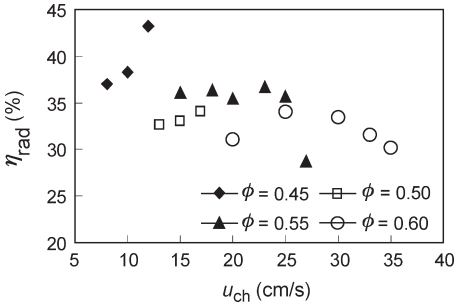

Figure 6. Radiation efficiency for pure methane as a function of the mean flow velocity for different equivalence ratios.

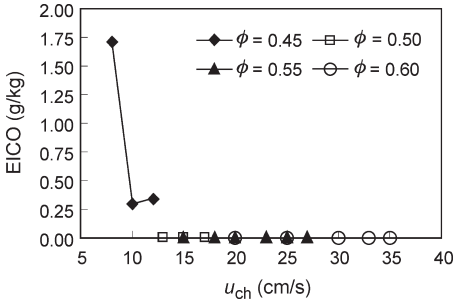

Figure 7. EI of CO for pure methane as a function of the mean flow velocity for different equivalence ratios.

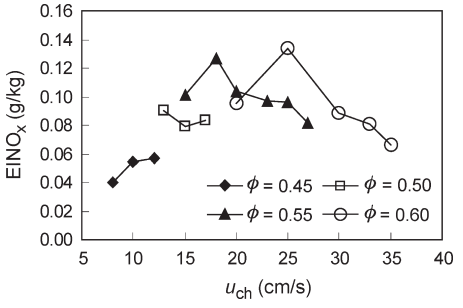

Figure 8. EI of NO_x for pure methane as a function of the mean flow velocity for different equivalence ratios.

mass of fuel burned and was calculated following the formulation described elsewhere.[42] The maximum EI of CO was 1.7 g/kg for a flame with $\phi = 0.45$ and $u_{ch} = 8$ cm/s. The temperature inside the porous burner increases with the equivalence ratio, which decreases the CO EI.

Figure 8 shows the EI of NO_x for pure methane as a function of the mean flow velocity for different equivalence ratios. The EI of NO_x varied between 0.04 and 0.13 g/kg. Because the temperatures increase with the equivalence ratio, the production of NO_x initially increases owing to the thermal mechanism (Zeldovich). However, further increases in the mean flow velocity cause a decrease in the NO_x production because of the lower residence times in the flame zone.

Figure 9 shows the EI of HC for pure methane as a function of the mean flow velocity for different equivalence ratios. Hydrocarbons may be formed because of the lower temperatures near the burner walls. The maximum HC EI was 0.08 g/kg for $\phi = 0.45$. The increase of the equivalence

(42) Turns, S. R. *An Introduction to Combustion—Concepts and Applications*, 2nd ed.; McGraw-Hill: New York, 2000; pp 553−554.

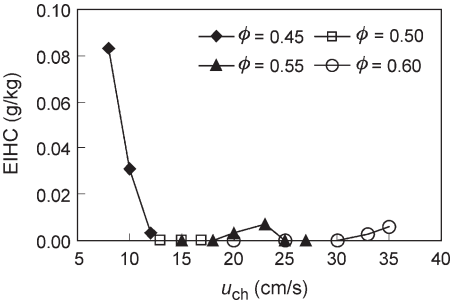

Figure 9. EI of HC for pure methane as a function of the mean flow velocity for different equivalence ratios.

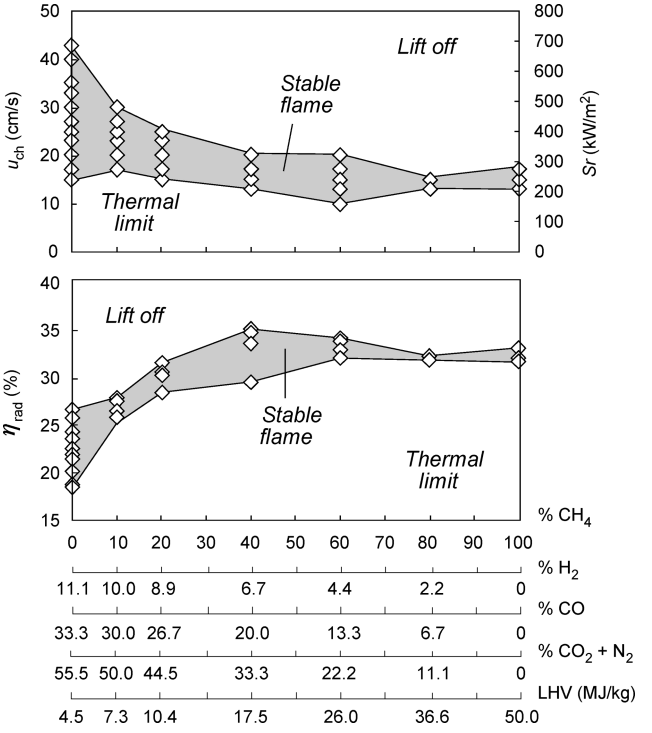

Figure 10. Flame stability limits and radiation efficiency for the fuel mixtures listed in Table 1 for $\phi = 0.5$.

ratio decreases the EI of HC because of the higher temperatures reached in the reaction zone.

3.3. Flame Stability Limits and Pollutant Emissions for Fuel Mixtures. Figure 10 shows the flame stability limits and radiation efficiency for the fuel mixtures listed in Table 2 for $\phi = 0.5$. Three different regions can be identified, namely, the lift off region, the stable flame region, and the region below the thermal damage limit.

The results provide evidence that, from 100 to 0% CH_4, the upper limit increases and the stability range enlarges. We note that the maximum burner power for 100% CH_4 was 1.08 kW (280 kW/m^2), while for 0% CH_4, it was 2.64 kW (685 kW/m^2), which is about 144% higher. For methane concentrations higher than 40%, the stability limits do not vary appreciably. We also note that, for WI varying from 5 to 44 (Table 2), it is possible to burn stably at around 1 kW (260 kW/m^2), showing the fuel interchangeability potential of the present burner design.

The range from lower to upper stability limits is determined by the flame position as it moves from the injection plate to the lift off condition. Here, the adiabatic flame temperature is approximately constant for all fuel mixtures

(Table 2). Therefore, the flame position is not influenced by the overall energy content of the reactant mixture but by the variation in consumption flame speed as the fuel composition changes. The laminar flame speed increases with the increase in H_2. The flame then penetrates deeper within the porous medium and stabilizes against higher mean flow velocities, which are closer to the distribution plate. This results in an increase of the upper stability limits.

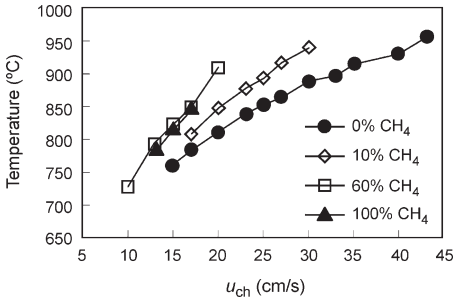

Figure 11. Surface temperature as a function of the mean flow velocity for different fuel mixtures for $\phi = 0.5$.

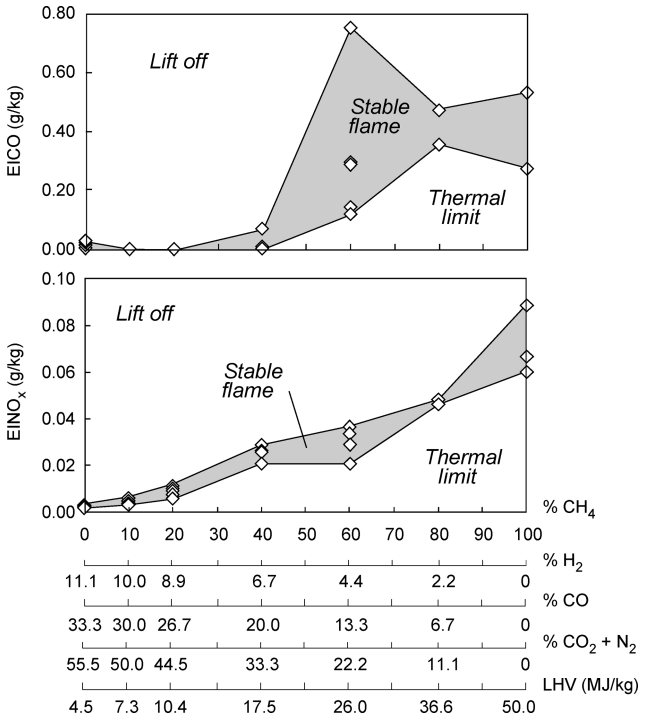

Figure 12. EI of CO and NO_x as a function of the chemical composition of the fuel mixture.

From the results of Figure 10, it can be noticed that, for 100% CH_4, the results of the maximum radiation efficiency obtained are situated above 30%. For the other fuels, as the flame front penetrates further upstream, the surface temperature decreases and, consequently, the radiation efficiency also decreases. Figure 11 shows the surface temperature as a function of the mean flow velocity for different fuel mixtures for $\phi = 0.5$. When the methane concentration is increased, the surface temperature increases for the same flow velocity. The results for fuel mixtures with the CH_4 concentration higher than 20% are closer to those for pure methane.

Figure 12 shows the EI of CO and NO_x as a function of the chemical composition of the fuel mixture. The pollutant EIs of HC were not significant, and the maximum value obtained was 0.02 g/kg.

In general, the EI of CO and NO_x increases as the CH_4 concentration increases. Although the NO emission increases monotonically, the CO emission presents a maximum at 60% CH_4. This effect is a result of the flame temperature, as influenced by the flame position, and mean flow velocity, influencing the mean residence time. The highest EI of CO was obtained for 60% CH_4, at $u_{ch} = 10$ cm/s, which was the lowest stable mean flow velocity obtained for all fuels (Figure 10). This trend is presented in Figure 13, which shows the EI of CO and NO_x as a function of the mean flow velocity for the different fuel mixtures. We note that, for both lower and higher mean flow velocities, the CO emission increases. A possible explanation for this observation is that, at lower u_{ch}, the flame burns closer to the injection plate. Although there is a longer residence time, the flame temperature is lower (Figure 14). Conversely, at higher u_{ch}, the flame burns closer to the outlet surface. In this case, the flame temperature is higher but the residence time is shorter. Both conditions lead to increased CO emissions. A similar trend is exhibited by the other fuel mixtures. In contrast, the NO EI decreases for both lower and higher velocities because of the same effects of flame temperature and residence time.

In summary, the maximum EI of CO was 0.75 g/kg for a flame with 60% CH_4 and $u_{ch} = 10$ cm/s. For NO_x, the maximum EI was 0.09 g/kg for a flame with 100% CH_4 and $u_{ch} = 15$ cm/s.

4. Conclusions

A range of low calorific value gaseous fuel mixtures containing CH_4, H_2, CO_2, CO, and N_2 have been burned in a porous radiant burner to analyze the effects of the fuel composition on flame stability and pollutant emissions. In the fuel mixtures studied, the CH_4 composition varied from 0 to 100% with the concentrations of the other gases varying in

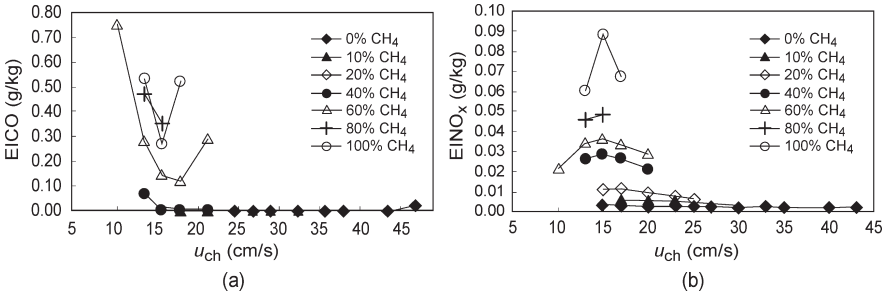

Figure 13. EI of (a) CO and (b) NO_x as a function of the mean flow velocity for the different fuel mixtures.

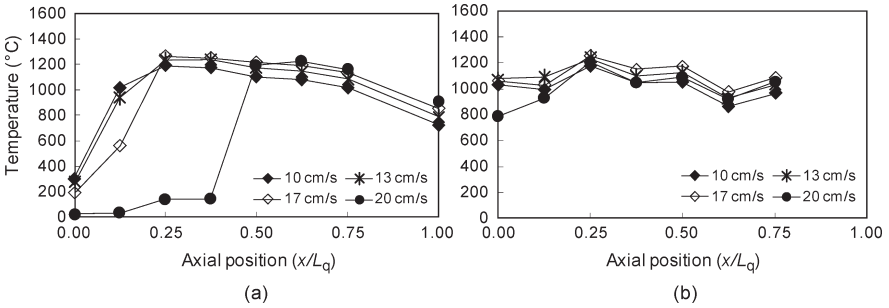

Figure 14. Temperature at the (a) burner centerline and (b) $R/2$ as a function of the axial position for different mean flow velocities for the fuel mixture with 60% CH_4.

such a way that the constant pressure adiabatic flame temperature for all reacting mixtures was kept constant. In this study, the equivalence ratio was also kept constant.

The results have indicated that the macroscopic flame shape of the fuel mixtures remains approximately the same as compared to pure methane but the former flames move further upstream from the burner exit. This is supposed to be caused by the increase of the laminar flame speed as the H_2 content in the mixtures increases. Predictions of the laminar flame speed with the available GRIMech 3.0[33] and Davis et al.[41] mechanisms using ChemKin 3.6[32] present the same trend, except for methane concentrations below 10%, for which the predicted laminar flame speed in fact decreases, even with the increase of the H_2 concentration. At the moment, we offer no explanation of this behavior, because an extensive sensitivity analysis is outside the scope of the present contribution. This range of stoichiometry, however, falls outside the optimization range for both mechanisms, and this result should therefore be used with caution. As a result, the stability limits of the fuel mixture increase and the stability range enlarges, which result in higher burner powers and a larger operation range. For the fuel with 100% CH_4, the maximum thermal power obtained was 280 kW/m^2, while for the fuel mixture with 0% CH_4, the maximum thermal power obtained was 685 kW/m^2, which is about 144% higher. We note that the calculated flame speed for 0% CH_4 was only 52% higher than for 100% CH_4. Also, the stability range enlarged from 13 to 17 cm/s (from 213 to 260 kW/m^2, 1.2 times) for a fuel with 100% CH_4 to from about 15 to 40 cm/s (from 239 to 639 kW/m^2, 2.7 times) for a fuel with 0% CH_4. It was also noted that, for WI varying from 5 to 44, it is possible to burn stably at ≈260 kW/m^2, which reveals the fuel interchangeability potential of the present burner design.

Because the flame moves further upstream, the enrichment with H_2 decreases the radiation efficiency. For pure CH_4, the radiation efficiency remained at about 35%. For the fuel mixture with 0% CH_4, the radiation efficiency varied between 18 and 26%.

The pollutant EIs decreased significantly with the use of H_2-enriched mixtures. For all fuel mixtures, the maximum EI of CO and NO_x was 0.75 and 0.09 g/kg, respectively.

Acknowledgment. This work was developed within the framework of Project PTDC/EME-MFE/67093/2006, which is financially supported by Fundação para a Ciência e a Tecnologia (FCT). The authors also acknowledge the Brazilian National Council for Research (CNPq) for the scholarship for R. C. Catapan.

Note Added after ASAP Publication. This article was published ASAP on December 30, 2009, with minor text errors. The correct version was reposted on January 4, 2010.